Materials Science and Engineering R 70 (2010) 320–329

Contents lists available at ScienceDirect

Materials Science and Engineering R

journal homepage: www.elsevier.com/locate/mser

Lateral nanowire/nanobelt based nanogenerators, piezotronics and piezo-phototronics

Zhong Lin Wang *, Rusen Yang, Jun Zhou, Yong Qin, Chen Xu, Youfan Hu, Sheng Xu

School of Materials Science and Engineering, Georgia Institute of Technology, Atlanta, GA 30332-0245, USA

ARTICLE INFO

Article history:
Available online 26 June 2010

Keywords:
ZnO
Nanowire
Nanogenerators
Piezotronics
Piezo-photonics
Piezo-phototronics
Self-powered nanodevices/nanosystems
Sensor network
Internet of things

ABSTRACT

Relying on the piezopotential created in ZnO under straining, nanogenerators, piezotronics and piezo-phototronics developed based on laterally bonded nanowires on a polymer substrate have been reviewed. The principle of the nanogenerator is a transient flow of electrons in external load as driven by the piezopotential created by dynamic straining. By integrating the contribution made by millions of nanowires, the output voltage has been raised to 1.2 V. Consequently, self-powered nanodevices have been demonstrated. This is an important platform technology for the future sensor network and the internet of things. Alternatively, the piezopotential can act as a gate voltage that can tune/gate the transport process of the charge carriers in the nanowire, which is a gate-electrode free field effect transistor (FET). The device fabricated based on this principle is called the piezotronic device. Piezo-phototronic effect is about the tuning and controlling of electro-optical processes by strain induced piezopotential. The piezotronic, piezophotonic and pieozo-phototronic devices are focused on low frequency applications in areas involving mechanical actions, such as MEMS/NEMS, nanorobotics, sensors, actuators and triggers.

Contents

1. Introduction

As important as carbon nanotubes and silicon nanowires, ZnO nanostructures are probably the most important one-dimensional oxide semiconductor for a wide range of applications [1,2]. ZnO nanostructures exhibit a range of interesting morphologies, such as nanowires (NWs)/nanobelts [3–6], nanosprings [7,8], nanorings [9], nanohelixes [10] and nanotubes [11]. ZnO NWs have been found to be mechanically robust [12], biocompatible and environmental friendly [13], which permit their applications in electronics, optoelectronics, biology and environmental science. The semiconducting and piezoelectric properties of ZnO make it ideal for ultraviolet (UV) lasering [14], light emitting diode [15,16], field emitter [17,18], UV sensor [19], gas sensor [20,21], solar cell [22], nanogenerator [23,24], and nanopiezotronics [25,26].

The first nanogenerator was demonstrated using a single ZnO NW in 2006 [23]. Later the DC nanogenerator was fabricated using vertically aligned NW arrays with the use of a zigzag electrode [24].

* Corresponding author.
E-mail address: zlwang@gatech.edu (Z.L. Wang).

0927-796X/$ – see front matter © 2010 Elsevier B.V. All rights reserved.
doi:10.1016/j.mser.2010.06.015

Following this pioneer work, nanogenerators toward high power output have been developed [27–29], with an output voltage of more than 1 V. The development of the nanogenerator using lateral NW whose both ends are fixed to the substrate is another milestone work [30], and a series of devices [31,32] have also demonstrated based on this approach. Reviews on the vertical nanowire based nanogenerators and nanopiezotronics have been published previously [1,25]. As a complimentary to the existing review, the current review focuses on the fundamentals and applications of nanogenerators and nanopiezotronics developed using laterally bonded ZnO nanowires/nanobelts.

2. Piezoelectric potential

The piezoelectric phenomenon is dictated by the crystal structure. ZnO has the wurtzite structure (Fig. 1a), in which the tetrahedrally coordinated O^{2-} and Zn^{2+} are stacked layer by layer along the *c*-axis. It has a hexagonal unit cell ($a = 0.3296$ and $c = 0.52065$ nm) with space group $P6_3mc$. The lack of the central symmetry of the wurtzite structure results in the piezoelectric property of ZnO, which is vital for the mechanic–electric energy conversion with the ZnO-based nanogenerator as well as the current modulation in the strain sensor and other devices [31,32].

The fundamental of the nanogenerator and nanopiezotronics relies on the presence of a piezoelectric potential (piezopotential) generated in a nanowire/nanobelt via dynamic straining. The cations and anions are tetrahedrally coordinated in the wurtzite-structured ZnO. At the strain free status, the charge-center of the cations and that of anions coincide with each other. When an external strain is applied, the structure is deformed so that the charge-centers of cations and anions separate and result in an electric dipole (Fig. 1c). Because the ionic charges are not free to move and the intrinsic free charge carriers can only partially screen them if the doping level is low, the piezoelectric field is preserved as long as the NW is strained. The potential created by the polar ions is called *piezoelectric potential*, or *piezopotential*.

The presence of piezopotential is the fundamental physical basis of the nanogenerators and piezotronics. When a strained crystal is connected to an external load, the electrons in the circuit are driven to flow to partially screen the piezopotential, which is the energy conversion process. Therefore, *the principle of the nanogenerator is the transient flow of electrons in external load as driven by the piezopotential created by dynamic straining* (Fig. 1c).

On the other hand, if the material is also a semiconductor, the piezopotential acts as a gate voltage that can tune/gate the transport process of the charge carriers under the driving force of an externally applied voltage (Fig. 1d). The device fabricated based on this principle is called the piezotronic device.

The piezopotential in a ZnO NW under different straining has been investigated using the perturbation theory and finite element method (FEM) [33–35]. As shown in Fig. 2a, the length of the nanowire is taken as 1.2 μm and the side length of the hexagon is 100 nm. At both ends, about 100 nm is preserved as the unstrained part that serves as the contacting part of ZnO NW with the electrode in a real device. When a uniform stretching force of 85 nN is applied along *c*-axis, the NW is elongated for 0.02 nm with a tensile strain of 2×10^{-5}. The piezopotential distribution can be obtained with FEM if we ignore the doping or conductivity in ZnO, as shown in Fig. 2b. The potential drop from the $+c$-axis side to the $-c$-axis side is approximately 0.4 V. When the NW is compressed with the same amount of force, the compressive strain becomes -2×10^{-5} and potential difference remains 0.4 V while the potential distribution is reversed with the $+c$-axis side having lower potential (Fig. 2c).

The above-calculated results need to be modified if we include the contribution made by the free charge carriers in the NW contributed by dopants or intrinsic defects. The intrinsic point defect in an as-grown ZnO NW always shows an n-type semiconducting behavior. The influence of the free charge carriers (electrons in an n-type ZnO NW) on the piezopotential has been investigated under a thermodynamic equilibrium condition [34]. Driven by the piezoelectric field, the free charge carrier will redistribute to tentatively screen the positive piezopotential zone. Considering the donor concentration to be around 10^{17} cm^{-3}, which is typical for an as-grown NW, the charge carriers will accumulate at the positive potential side ($+c$-axis side in a stretched NW or $-c$-axis side in a compressed NW) and the negative potential side is not significantly affected. As a result of this charge redistribution, the positive potential is clearly screened while the negative potential region is still preserved. The negative piezopotential in the NW can be effective for nanogenerator and piezotronics.

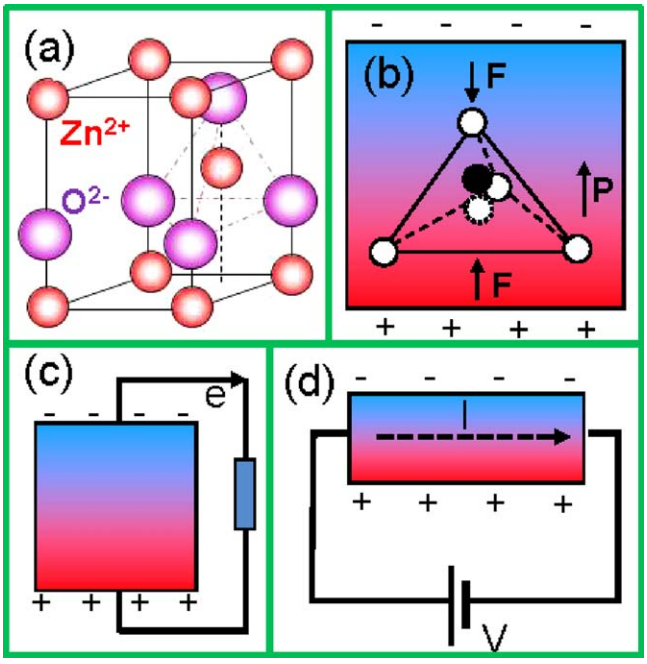

Fig. 1. (a) Atomic model of the wurtzite-structured ZnO. (b) Piezopotential of a stretched ZnO nanowire. (c) Power generation with the piezopotential. (d) Current modulation in a semiconductor material by the piezopotential.

3. Single wire generator

3.1. Piezopotential-driven transient flow of electrons in an external load is the principle of the nanogenerator

Fig. 3 presents a single wire generator (SWG) using a laterally packaged ZnO wire. A microwire is used in the study of the first

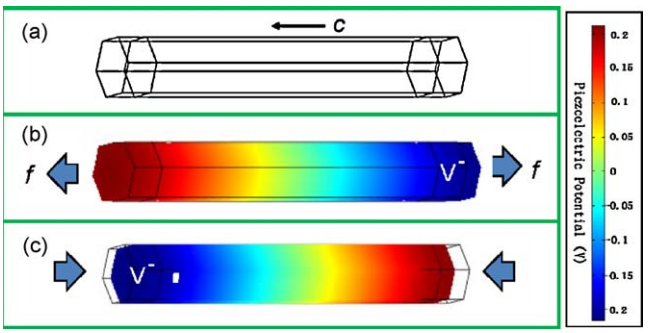

Fig. 2. Numerical simulation of the piezopotential distribution in an insulating ZnO nanowire. (a) The piezopotential distribution and the deformed shape of a ZnO nanowire grown along *c*-axis under a stretching force of 85 nN (b), or a compressing force of 85 nN (c) (from Ref. [35]).

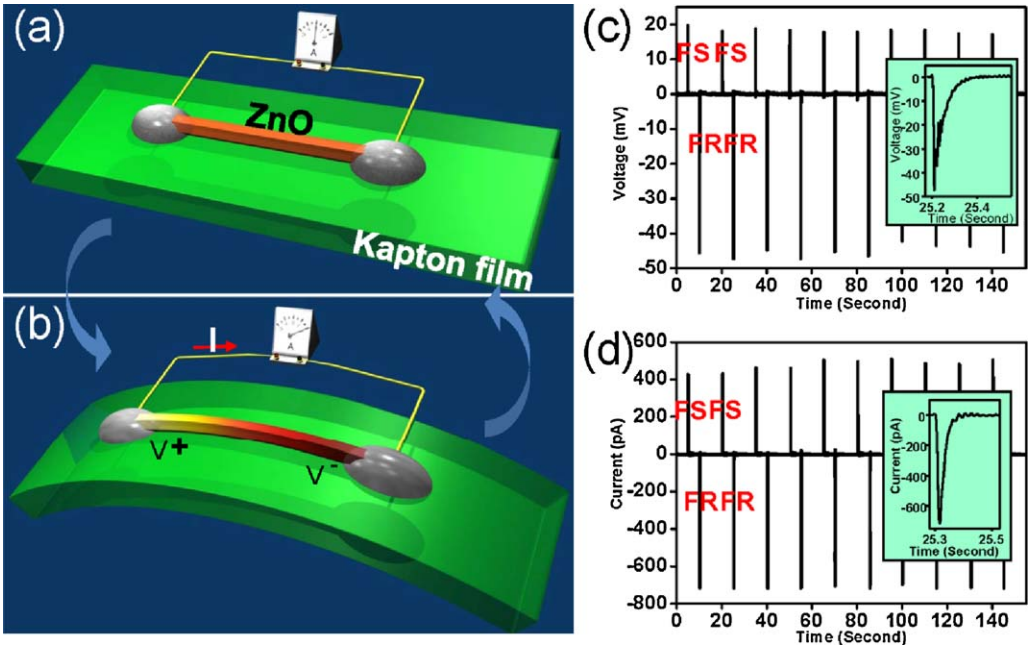

Fig. 3. Design and power output from a single wire generator. (a and b) Schematic diagram of single wire generator before and after stretching. Open-circuit voltage (c) and short-circuit current (d) of the single wire generator, which was cyclically fast stretched and fast released (from Ref. [30]).

SWG for easy demonstration, although nanowires can function in the same way and has also been used for the fabrication of the SWG. The detailed fabrication is given in [30]. In brief, a single ZnO wire was placed laterally on the flexible polyimide film. Silver paste can be used to fix two ends of the ZnO wire to the substrate and link the wire to the external measuring instrument through metallic wires. Electric measurement shows that a functioning SWG usually has rectifying *I–V* characteristic, indicating the existence of the Schottky contact at least at one end. Before we deform the SWG, there is no measureable potential drop from the ZnO wire. When we bend the substrate, both the substrate and the ZnO wire are under strain. Because the thickness of the substrate is much larger than the dimension of the ZnO wire, the ZnO wire is experiencing solely tensile strain when the bend is concave downward, as shown in Fig. 3b. As discussed earlier, tensile strain will result in piezopotential, such that the +*c*-axis side gains positive potential (light yellow) and −*c*-axis side gains negative potential (dark red). The potential difference between the two ends can then be measured as either open-circuit voltage (Fig. 3c) or short-circuit current (Fig. 3d).

When the SWG is cyclically fast stretched (FS) and fast released (FR) with the maximum strain around 0.05–0.1%, the generated open-circuit voltage reaches 20–50 mV and the closed-circuit current reaches 400–750 pA. The mechanical energy is converted into electricity through the piezoelectric wire with a conversion efficiency of 7% if only the wire is considered. The different peak height corresponding to FS and FR are mainly due to different strain rate, which is further confirmed with controlled measurements at different strain rate. Although the peak height is different, the areas under the current are the same (within 5%) for FS process and FR process. In other words, the same amount of charge carriers flew through the external circuit for both processes, which are the result of conservation of charges.

The working mechanism of the SWG can be understood with the energy band diagram in Fig. 4. The Schottky contact at least at one end is necessary for the energy generation. For easy discussion, the Schottky contact is assumed at the +*c*-axis side (left side in Fig. 4a), and the energy generation follows a similar way when the Schottky contact is at the other side or both sides. The entire wire is in equilibrium state without any strain and power output (Fig. 4a

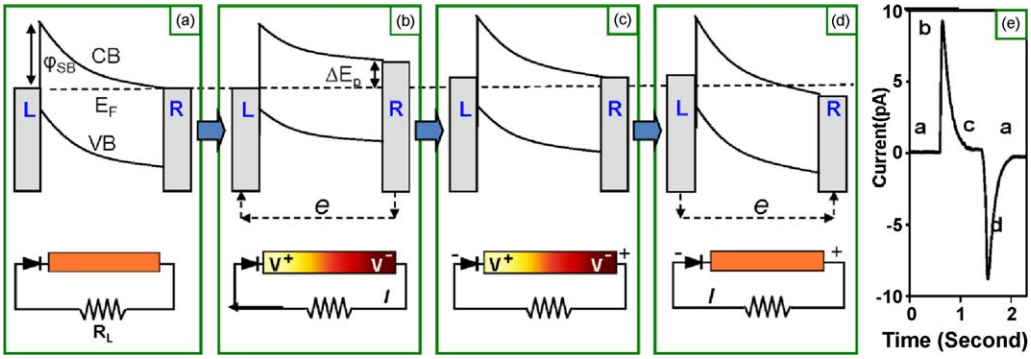

Fig. 4. Current generation mechanism explained with energy band diagram of the cyclically stretched NW. Energy band diagram of the ZnO NW in equilibrium and free condition (a), non-equilibrium and tensile strained condition (b), re-reached equilibrium and tensile strained condition (c), and non-equilibrium and free condition (d). After (d), the NW will reach equilibrium as in (a) after charges flow. E_F, CB, VB, Φ_{SB}, and ΔE_p indicate Fermi level of the electrode, conduction band and valence band of ZnO, Schottky barrier height, and piezopotential difference, respectively. (e) Short-circuit current measurement in which the labels of a, b, c, and d indicate the corresponding process shown in subparts a–d (from Ref. [30]).

an e). When the wire is stretched, the tensile strain induces polarization of ions and the piezoelectric field. Consequently, the +*c*-axis side holds positive potential and the −*c*-axis side is negative potential, with a potential difference of ΔE_p. The conduction band edge and the Fermi level of the right-hand side electrode are raised for the same amount of ΔE_p. The electrons in the external circuit should flow from the right-hand side to the left-hand side to compensate the energy difference, which will generate the first output signal if the flow rate is sufficiently large, as indicated in Fig. 4b and e. The electrons cannot flow across the interface through the wire due to the presence of a threshold potential, thus, they tend to flow through the external load to reach the left-hand side electrode, but they cannot across the interface due to the presence of the Schottky barrier. When the electrons and the piezoelectric field reach equilibrium, the Fermi energy on both sides is on the same level and there is no more current flow (Fig. 4c and e). When the SWG is fast released, there is no strain inside the NW. As a result, the polarization and piezoelectric field vanish as well and the equilibrium with the accumulated electrons is broken. The accumulated charge carriers flow back from the left-hand side to the right-hand side through the external circuit, producing the second output signal in the opposite direction, as shown in Fig. 4d and e.

This working mechanism enables the SWG to harvest mechanical energy from a wide range of sources as long as there are mechanical instability and fluctuation. A living species has abundant sources of mechanical energy, such as walking, breathing, and heart beating. A wide range of fluctuation in frequency and intensity is a challenging issue. This issue seriously retarded the progress of energy harvesting using traditional techniques. Our approach provides a new technology for harvesting mechanical energy from irregular motion with a magnitude at very gentle level without adding any appreciable burden.

The first example of the biomechanical energy harvesting was a SWG driven by a human finger [36]. The NW in the SWG was 100–800 nm in diameter and 100–500 μm in length. A flexible polymer layer over the entire SWG improved its robustness and adaptability. The SWG was affixed at the joint position at the top of an index finger, as shown in the inset in Fig. 5a. The tapping of the finger induced the deformation of the ZnO NW in the SWG with a strain rate about $4–8 \times 10^{-3}\ s^{-1}$ and a maximum strain of ~0.2%. As discussed earlier, the strain results in a piezoelectric polarization along the NW and thus a potential difference between the two ends, which droves the flow of the electrons in the external circuit. Such physical motion is a very gentle and slow motion.

The measured open-circuit voltage and closed-circuit current are presented in Fig. 5a and b, respectively. The periodic peaks are corresponding to the periodic tapping of the finger. Fig. 5a shows that the voltage output is up to 25 mV while the current from Fig. 5b can be more than 150 pA from a single SWG device.

In addition to the human finger, a living hamster has also been demonstrated to produce electricity with a SWG [36]. The hamster adopted in this experiment belongs to the Campbell's dwarf type, which can produce both regular and irregular motion, like running or scratching. A special jacket has been made for the hamster to wear such that the hamster could move freely in a round cage and drive the SWG on the jacket at the same time. We measured the electric output signal from the SWG without disturbing the movement of the hamster, as shown in Fig. 5c–e. Varied motion, running or scratching, of the hamster provided mechanical energy with distinct pattern and energy intensity to the SWG. As expected, the output electricity from the SWG changed as well. The enlarged voltage output signal in Fig. 5d from a running hamster shows a clearly periodic pattern with the magnitude about 50–100 mV and the frequency of ~10–11 Hz. This periodicity agrees well with the running steps of the hamster. The much higher signal than the

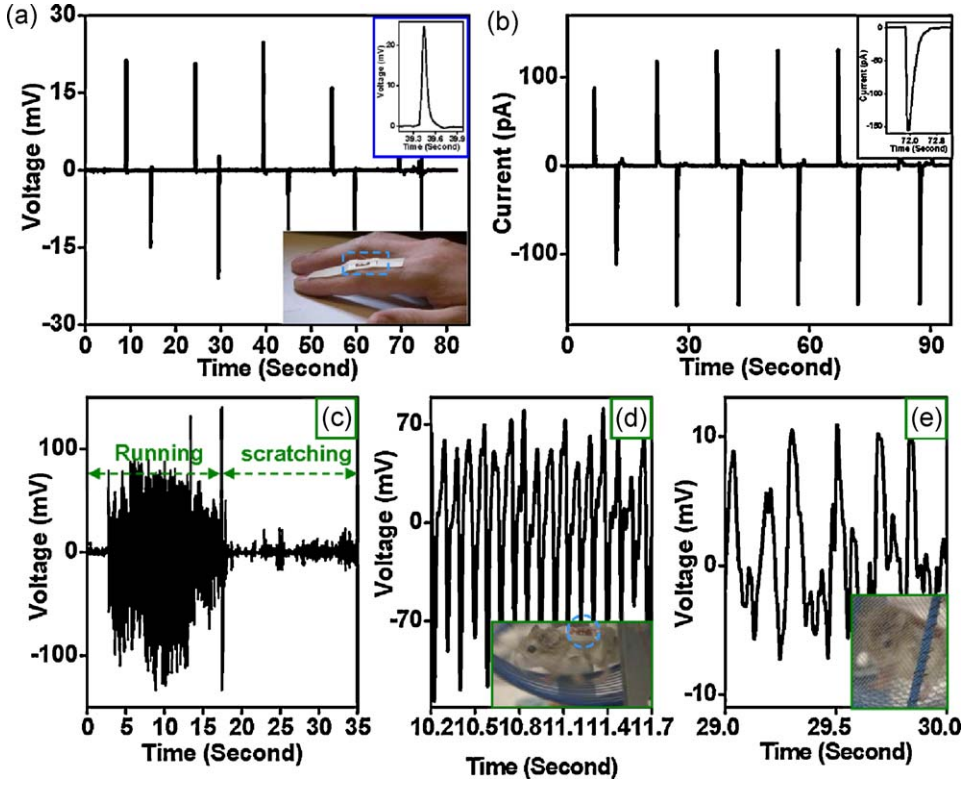

Fig. 5. Energy harvesting from biosystem with the nanogenerator. (a) Open-circuit voltage and (b) short-circuit current output from a single wire generator fixed at the top of the index, as shown in the inset. (c) Open-circuit voltage output from a nanogenerator fixed to the jacket worn by a hamster while it's running or scratching. (d) and (e) are enlarged voltage output corresponding to the running hamster and scratching hamster, respectively. Insets in (d) and (e) are corresponding snapshots of the hamster with the nanogenerator on its back (from Ref. [36]).

SWG on the human finger is due to the much faster strain rate of the running hamster. In comparison, the voltage output from a scratching hamster, as shown in Fig. 5d, was quite irregular with lowered magnitude due to the irregular movement and less intense activity of the hamster. The closed-circuit current measurement revealed similar phenomena. A running hamster produced a periodic alternating current up to ~0.5 nA and a scratching hamster produced a lower irregular current.

Integration of SWGs is a major step towards the practical applications. Taking advantage of the small size of the NW, we can put multiple SWGs on a single substrate such that the hamster can drive all SWGs simultaneously. Integration of up to four SWGs in serial has been demonstrated with the open-circuit voltage of ~0.1–0.15 V. The output current can also be improved with multiple SWGs in parallel. The work on the human finger and living hamster clearly demonstrated the capability of the SWG to scavenge mechanical energy from the biosystem. It also confirmed the feasibility of using the SWG for harvesting the energy created by regular and irregular motions.

4. Criteria for identifying the true output signals from a nanogenerator

Since the output signal from a nanogenerator is usually small. It is easy to confuse the true signal with artifacts arising from the measurement system, parasitic capacitance, or resistance change in the circuit. In order to identify the true signal generated from the device and rule out any artifact or noise, we have developed three criteria with 11 measurements [37]. The first criterion is the non-linear (Schottky) behavior in the *I–V* measurement. The Schottky contact at the interface can effectively regulate the flow of electrons in the external circuit. In comparison, a device with only linear Ohmic contact at both ends cannot effectively produce power output. This criterion greatly facilitates the elimination of the defective devices. The second criterion is called switching-polarity test with two measurements. We achieved positive and negative peaks when we bent and released the nanogenerator, respectively, in Fig. 3c for open-circuit voltage and in Fig. 3d for short-circuit current. When we reverse the connecting polarity of the nanogenerator to the measurement system, the true signal should be reversed in sign, which was exactly what we have observed. Due to the bias current from measurement system and other environmental influences, the signal magnitude after reversing the device might not remain the same. However, the reverse of the signal after reversing the device is required to ensure that the measured signal is truly from the nanogenerator.

Due to the asymmetric Schottky contact, the above two criteria are necessary but not sufficient to confirm the source of the measured signal. Consequently, we added the third criterion, linear superposition tests with eight configurations for both voltage and current measurement. We have two nanogenerators, namely *A* and *B*. First we need to measure the open-circuit voltage and short-circuit current from both nanogenerators. The measured results are defined as V_A^+, V_B^+, I_A^+, and I_B^+ corresponding to the configurations in the first row from left to right in Fig. 6a. For the purpose of simplicity, we adopted the logo designed in [37] to represent the piezoelectric nanogenerator. We then need to reverse the device such that the two probes from the measurement instrument

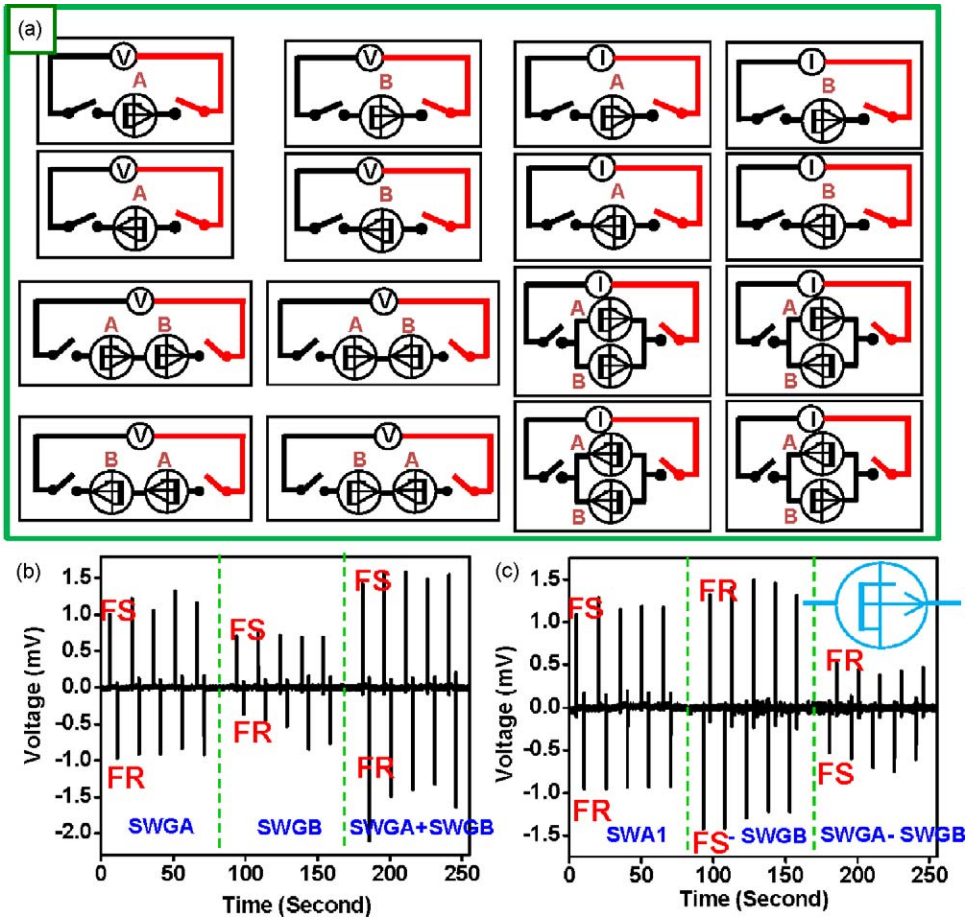

Fig. 6. (a) Measurement configurations for the linear superposition tests. Voltage output from two single wire generators independently and connected in serial (b), or anti-serial (c) (from Refs. [30,37]). The inset in (c) is the designed logo for the piezoelectric nanogenerator.

exchange their connections to the leading wires of the nanogenerator. The measured result in these configurations in the second row from left to right in Fig. 6a are defined as V_A^-, V_B^-, I_A^-, and I_B^-. Finally we need to connect these two nanogenerators in serial, anti-serial, parallel, and anti-parallel, as illustrated in the last two rows in Fig. 6a. If we define the measured result as V_{A+B}^+, V_{A-B}^+, I_{A+B}^+, and I_{A-B}^+, in the third row and V_{A+B}^-, V_{A-B}^-, I_{A+B}^-, and I_{A-B}^- in the fourth row, the linear superposition adds the following requirements for open-circuit voltage

$$V_{A+B}^+ = V_A^+ + V_B^+, \quad V_{A+B}^- = V_A^- + V_B^-, \quad V_{A-B}^+ = V_A^+ + V_B^-, \quad V_{A-B}^- = V_A^- + V_B^+$$

and requirements for short-circuit current

$$I_{A+B}^+ = I_A^+ + I_B^+, \quad I_{A+B}^- = I_A^- + I_B^-, \quad I_{A-B}^+ = I_A^+ + I_B^-, \quad I_{A-B}^- = I_A^- + I_B^+$$

The fundamental idea of this linear superposition criterion is testing the successful add up or cancel out of the integration of multiple nanogenerators. Fig. 6b and c presents an example for the voltage measurement of two SWGs [30]. In this example we can clearly see that the voltage adds up when those two SWGs are connected constructively in serials and cancels out when those two SWGs are in anti-serials. On the contrary, the noise and artifact cannot consistently add up or cancel out in those well-designed connection configurations.

Those three criteria are very important and necessary for the investigation of nanogenerators. The linear superposition also forms the fundamentals for the design and integration of the nanogenerators. Furthermore, those criteria and configurations can serve as standard tests for general purpose and benefit the investigation of all other types of energy harvesters.

5. Mega-nanowire integrated nanogenerator with high output

ZnO can be easily grown into vertically aligned NW arrays through a wet chemical approach [38] or physical vapor deposition process [39]. The fabrication relies on the manipulation of microwire/nanowires with probe station under a microscope. In comparison, the growth technique for laterally aligned ZnO nanowire arrays can significantly simplify the fabrication process of devices with lateral configuration and make the large-scale fabrication possible. Fig. 7 presents two wet chemical growth approaches for well aligned lateral ZnO NW arrays [40,41]. The detailed growth parameters can be found in [40,41]. The key for the lateral growth in Fig. 8a and b is the shielding layer on the top surface of the ZnO seed layer. The NW is only initiated and grows on the side wall, which is exposed to the nutrient solution. The selective growth on the side wall results in the laterally aligned ZnO NW arrays. The second approach in Fig. 7c–e takes the advantage of the single-crystalline ZnO substrate, which can initiate epitaxial growth of ZnO. The substrate was spin coated with a thin layer of polymethyl methacrylate (PMMA). Electron beam lithography (EBL) was employed to fabricate strip shape areas. The ZnO can easily nucleate and grow on those opened strip area. Fig. 8c presents laterally aligned ZnO NW arrays, which were grown from stripe areas of 2 μm by 400 nm each. The dimension of the ZnO nanowire can be easily tailored by the opening size of strips, as shown by the thick (Fig. 7d) and thin (Fig. 7e) ZnO nanowires.

A mega-nanowire integrated nanogenerator has been fabricated, as shown in Fig. 8 [42]. A non-symmetric Cr and Au electrodes were first designed to form arrayed structures. On the surface of the Cr electrodes, ZnO NWs were grown in parallel to the substrate (Fig. 8a). By depositing Au at the other end, a row of ~20,000 NWs in parallel connection were in electrical contact

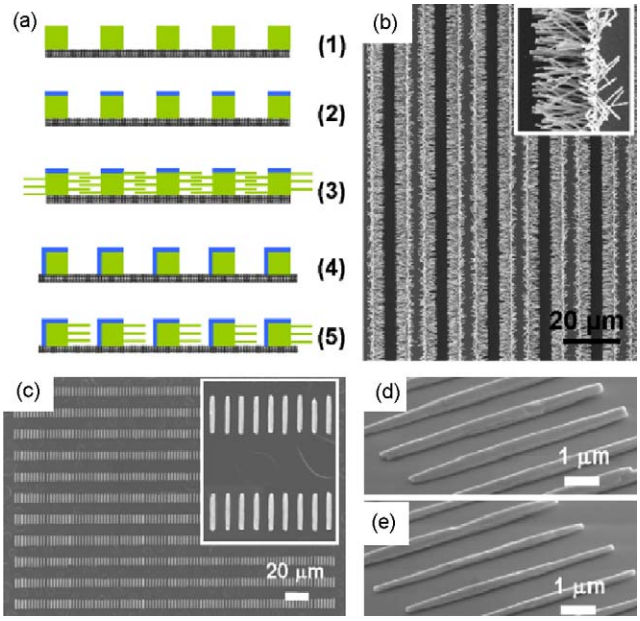

Fig. 7. (a) Flow chart of the laterally aligned NW growth with shielding layer and seed layer. (b) SEM image of ZnO NW arrays grown from (a). Enlarged view is given in the inset. (c) Laterally aligned ZnO NW arrays grown from single-crystalline ZnO substrate patterned with PMMA. Enlarged view is given in the inset. Thick (d) and thin (e) ZnO NW arrays controlled by the size of the openings of PMMA pattern (from Refs. [40,41]).

(Fig. 8b). A total of 700 rows have been integrated together form a structure shown in Fig. 8c. When the substrate was mechanically deformed, the LING has demonstrated an average output voltage of ~1.2 (Fig. 8d) at a straining rate of 2.13%/s and strain of 0.19%. If we excluded the area occupied by the electrodes, a peak output power density of ~70 nW/cm^2 was obtained. This is a landmark step toward high output nanogenerators. The approach demonstrated here establishes the technological road map for technological applications.

6. Piezotronic effect

As pointed out earlier in this paper, the strain-induced piezopotential can not only be used for energy generation, but also tune the current following through a semiconductor nanowire. The sensitive response of the transport behavior of ZnO nanowires to the external strain has been used for the fabrication of a series of devices. All of those devices follow the same fundamental principle and form a new type of device family, i.e. piezotronics [25,26].

Fig. 9 shows how the strain affects the electric property of the device consisting of a ZnO nanowire and silver electrodes [31,32,35]. Before the device experiencing any strain, the *I*–*V* curves showed a non-linear but roughly symmetric behavior in Fig. 9a. After the device was stretched, the *I*–*V* curve became non-symmetric. Tensile strain and compressive strain-induced opposite turn-on bias and polarity. In comparison, the device in Fig. 9b showed a rectification behavior before it was strained. When the device was stretched or compressed, the *I*–*V* behavior changed as well. With the same forward bias, the tensile strain increased the current while the compressive strain decreased the current. In addition, piezoelectric effect can also turn an Ohmic transport characteristic into a diode characteristic.

The distinct effect of the strain on the transport property can be understood using the energy band diagram. Strain can cause two effects on carrier transport: piezoresistance effect and the piezoelectric-field effect. The piezoresistance is about the change

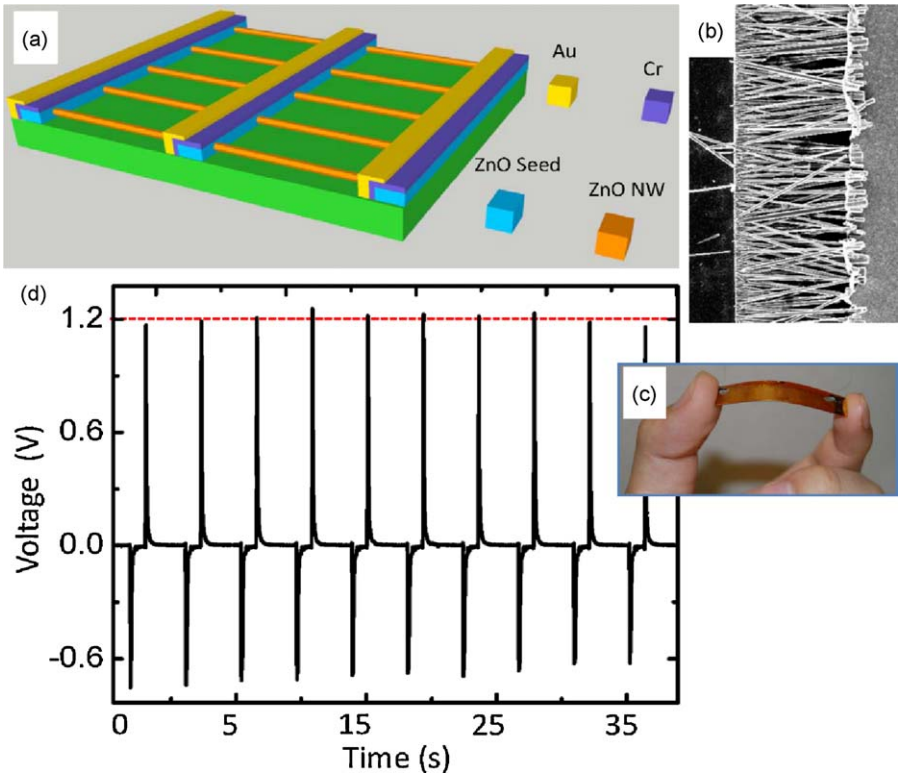

Fig. 8. (a) Schematic of laterally integrated nanowire generator (LING). (b) SEM image of a row of laterally grown ZnO NW array. (c) Optical microscopy image of a LING structure using 700 rows of NW arrays. (d) Open-circuit output voltage from a LING structure that is made of 700 rows of NW arrays. The maximum output voltage peak reaches 1.26 V (from Ref. [42]).

in conductance of the entire wire as the band structure being modulated by strain. If the NW experiences a uniform strain, no matter tensile strain or compressive strain, the uniform change of the bandgap raises or lowers the Schottky barrier height by an equal amount at both ends. Consequently, the piezoresistance effect is a symmetric effect at the two ends and it cannot explain the transition of symmetric *I–V* characteristic into a rectifying behavior as observed experimentally. However, the piezoelectric-field effect is

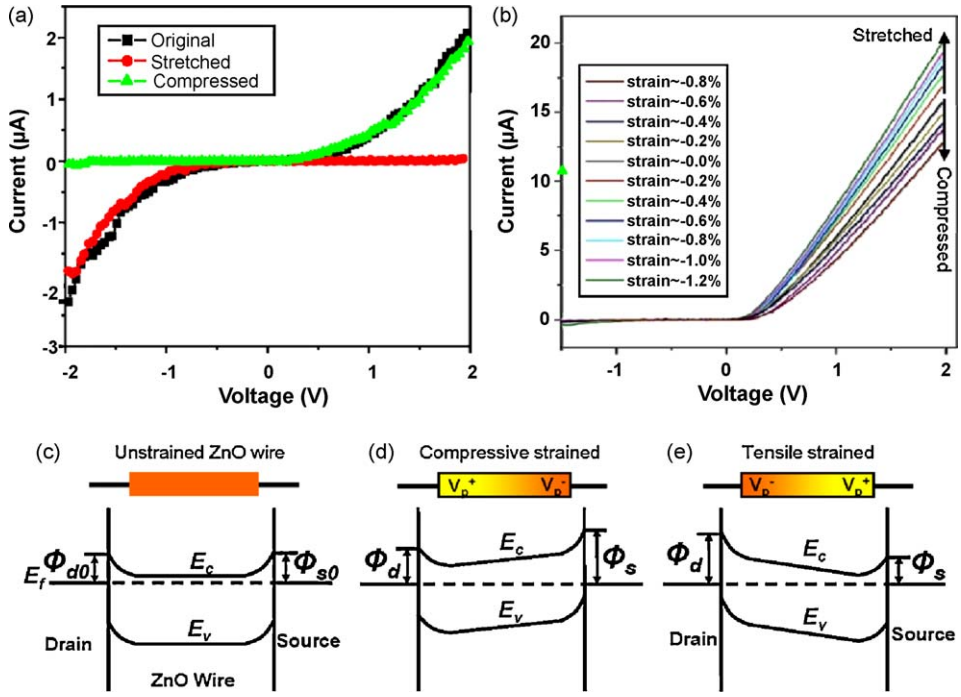

Fig. 9. Piezotronic effect. (a) Changes of the *I–V* characteristic of a ZnO NW from symmetric (black) to asymmetric rectifying behavior when it's stretched (red) or compressed (green). (b) Change of *I–V* characteristic of a ZnO NW with rectifying behavior when it's stretched or compressed. Schematic energy band diagram of the unstrained (c), compressive strained (d), and tensile strained (e) NW, showing the different effect of the piezopotential on the Schottky barrier height at drain electrode side and at source electrode side (from Ref. [31,32,35]). (For interpretation of the references to colour in this figure legend, the reader is referred to the web version of the article.)

not symmetric at the two ends, and it is main responsible to the observed piezotronic effect.

Fig. 9c present the schematic energy band diagram of the unstrained NW with *c*-axis of ZnO pointing towards the source. The Schottky barriers, Φ_{d0} and Φ_{s0}, at the source and drain respectively, are approximately the same, which result in a symmetric *I–V* characteristic behavior before any strain. When the NW is stretched or compressed, the cations and anions of the NW will be polarized. Those ionic charges cannot move freely and the piezoelectric field can only be partially screened by the free charge carriers within the NW. The remaining piezoelectric field inclines the conduction band and valence band of the semiconducting ZnO, such that the Schottky barrier height at the drain side, Φ_d, and Schottky barrier height at the source side, Φ_s, are changed by the same amount but in opposite directions, as shown in Fig. 9d for NW under compressive strain and in Fig. 9e for NW under tensile strain. Now the Schottky barrier heights are different at the two ends. Because the reverse-biased Schottky contact consumes the majority of voltage drop of the entire device according to the in situ scanning surface potential microscopy measurement [43], the non-symmetric Schottky contacts at the two ends change the symmetric *I–V* characteristic into a non-symmetric behavior, as demonstrated in Fig. 9a. Alternatively, if the starting device has non-symmetric Schottky barrier height at two ends, the strain can still tune the *I–V* characteristic with the modulation of the barrier in different way at two ends (Fig. 9b). If the starting device has no barrier at the end and shows a linear behavior in the *I–V* characteristic, the inclined band structure of ZnO due to piezopotential can induce a raise of barrier height at one end and result in a non-linear *I–V* characteristic.

The current through the NW is extremely sensitive to the Schottky barrier height, which can be further modified by the strain due to the piezoelectric effect. The coupling of the semiconducting and piezoelectric property is responsible for the new phenomena described above and has been utilized for the fabrication of many devices, such as piezoelectric diodes [31] and strain sensors [32].

7. Piezo-phototronic effect

The piezoelectric effect tends to raise the height of the local Schottky barrier (SB) at the ZnO–metal contact, while the photoexcitation lowers the SB height using a light that has energy higher than the bandgap of ZnO. The height and width of the SB have been modified by laser excitation due to the creation of local electron–hole pairs as well as the charge separation at the barrier, which can be effectively represented by a change in barrier height (see Fig. 10). By tuning the relative contributions of the effects from piezoelectricity via strain and photoexcitation via light intensity, the local contact can be tuned step-by-step and/or transformed from Schottky to Ohmic or from Ohmic to Schottky. Fig. 10 shows a schematic diagram about the three-way and two-way coupling among piezoelectricity, photoexcitation and semiconductor, which are basis of piezotronics (piezoelectricity–semiconductor coupling), piezo-photonics (piezoelectric–photon excitation coupling), optoelectronics, and piezo-phototronics (piezoelectricity–semiconductor–photoexcitation). The band diagram represents the tuning effect on the local Schottky contact by piezopotential or photon excitation. Piezo-phototronics can be a case of using strain/stress to tune the output of a photovoltaic [44] and LED.

The localized coupling among the piezoelectric, photoexcitation and semiconductor properties of a ZnO microwire/nanowire device has been studied for designing and controlling the electrical transport characteristics of the device [45]. As demonstrated in Fig. 2, strain can effectively increase the height of the Schottky barrier in ZnO wire based device, allowing a fine tuning of the electric transport property of the device. In contrast, the effective height of the Schottky barrier can be lowered by shining a laser beam at the local contact with excitation energy larger than the bandgap (see Fig. 10), which increases the density of the local electron–hole pairs and the change of barrier profile due to charge separation/redistribution. By controlling the magnitude of the strain and the intensity of the laser beam, we can effectively tune the charge transport property from Schottky to Ohmic or from

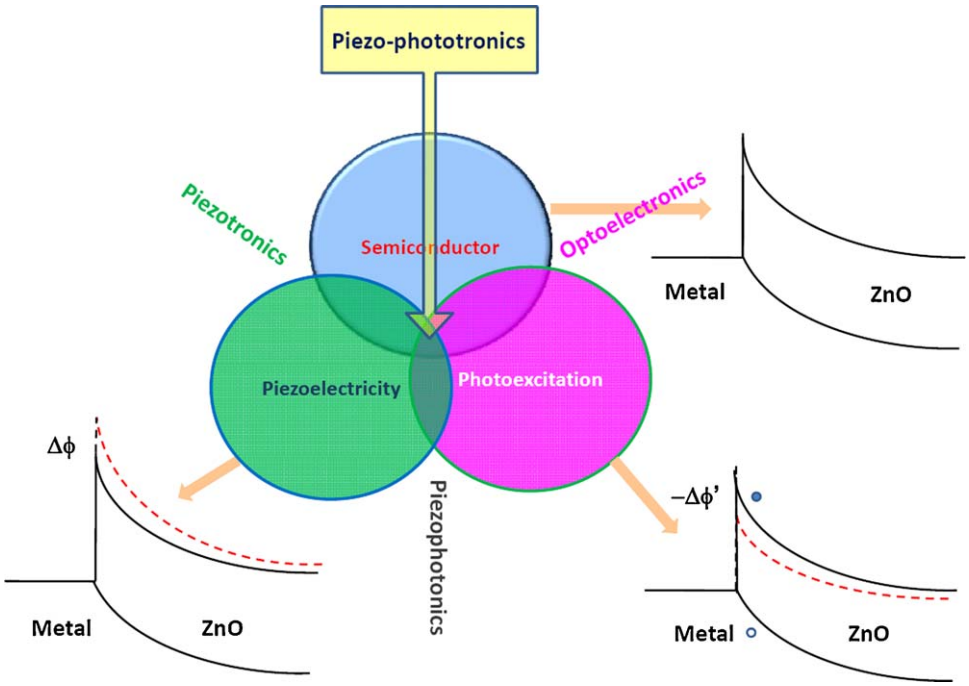

Fig. 10. Schematic diagram showing the three-way coupling among piezoelectricity, photoexcitation and semiconductor, which is the basis of piezotronics (piezoelectricity–semiconductor coupling), piezo-photonics (piezoelectric–photon excitation coupling), optoelectronics, and piezo-phototronics (piezoelectricity–semiconductor–photoexcitation). The core of these coupling relies on the piezopotential created by the piezoelectric materials. Wurtzite structures with finite conductivity area ideal for these applications.

Ohmic to Schottky. This study describes a new principle for controlling the coupling among mechanical, photonic and electrical properties of ZnO nanowires, which can be the basis for fabricating piezo-photonic–electronic nanodevices. Therefore, *piezo-phototronic effect* is about the tuning and controlling of electro-optical processes by strain-induced piezopotential [45].

To illustrate the piezo-phototronic effect, we have fabricated a two-end bonded ZnO wire device. Owing to the variation in local contacts, the device shows an asymmetric *I–V* transport property. Both piezoelectric effect and photoexcitation intensity can tune the *I–V* transport property of a ZnO microwire device, but they act in opposite directions. If we refer one end of the device as A, by shining the laser at contact A of the device, as the relative intensity of the light being changed via optical filters from transmission coefficient $T = 0.001$ to $T = 1$, the *I–V* curve has been largely tuned (Fig. 11a). Fine tuning of the magnitude of mechanical straining and the intensity of the light illumination can produce a designed shape of the *I–V* characteristic. Fig. 11b shows the coupled tuning of the two effects on the *I–V* shape. By choosing a strain of −0.2% and relative light intensity $T = 0.01$ (green curve), the observed *I–V* curve matched well to the original *I–V* curve obtained without applying a strain nor laser excitation (dark curve). This experiment shows the possibility of controlling the *I–V* characteristic of a nanowire device by piezo-phototronic effect [45].

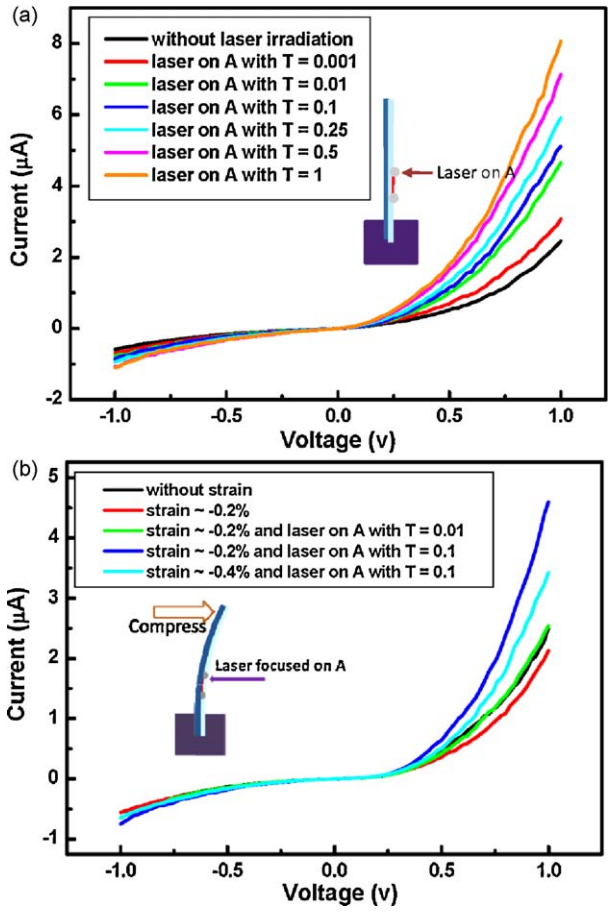

Fig. 11. Piezo-phototronic effect by coupling among piezoelectric, photon excitation and semiconductor properties. (a) Tuning the *I–V* transport characteristic of a device by controlling the intensity of the excitation laser focused at contact A via optical filters from transmission coefficient $T = 0.001$ to $T = 1$, without strain. (b) Design and control the transport properties of the device by coupling the intensity of illuminating laser and the degree of straining in the microwire showing the basic principle of piezo-phototronics (from Ref. [45]). The insets are the corresponding configurations of the two-end bonded nanowire device.

8. Summary

ZnO nanomaterials have been widely studied and various applications have been demonstrated. Relying on the piezopotential created in ZnO under straining, nanogenerators, piezotronics and piezo-phototronics have been demonstrated. The principle of the nanogenerator is a transient flow of electrons in external load as driven by the piezopotential created by dynamic straining. Alternatively, the piezopotential can act as a gate voltage that can tune/gate the transport process of the charge carriers in the nanowire, which is a gate-electrode free FET. The device fabricated based on this principle is called the piezotronic device. Piezo-phototronic effect is about the tuning and controlling of electro-optical processes by strain-induced piezopotential.

As one of the most important nanomaterials, ZnO has the following unique characteristics:

1. ZnO nanostructures exhibit extremely high elasticity and resistance to fatigue due to the small size and single crystallinity, which are important for the lifetime of the devices. [12]
2. The high power density of ZnO demonstrated in the nanogenerators reveals a great application in sustainable self-sufficient energy for micro- and nano-systems.
3. The coupling of piezoelectric and semiconducting properties, i.e. piezotronic effect, set the fundamental for a new field: piezotronics. A variety of devices, such as the nanogenerator, diode, and strain sensor, have been demonstrated.
4. The coupling of piezoelectric, optical, and semiconducting properties of ZnO, which can be named as piezo-phototronic effect, can initiate another interesting topic: piezo-phototronics.
5. The advance of the low-cost and controlled growth of ZnO nanowires on any shape and any type of substrates sets the solid foundation for the design, fabrication, and commercialization of novel devices in large scale.
6. Researchers have proved that the ZnO nanowires are biocompatible and environmental friendly.

With above listed figure of merits, combined with the unique phenomena and novel devices discovered to date, ZnO nanomaterials are important for future technology. This article mainly reviewed the principle and advances in devices based on ZnO nanowire/nanobelt in lateral configuration. The working principle is based on the piezopotential along the length. Both ends of the NW are fixed to the substrate and connected to the electrodes, which eliminates the wearing, deterioration, and other issues caused by the transient contact between the electrode and NWs as for energy conversion applications. Besides ZnO, materials in the wurtzite family, such as GaN [46] and InN [47] with output voltage of up to 1 V, are ideal candidates for the proposed devices.

The piezotronic and pieozo-phototronic devices are focused on low frequency applications in areas involving mechanical actions, such as MEMS/NEMS, nanorobotics, sensors, actuators, triggers and self-powered nanosystems. The speed offered by piezotronic and pieozo-phototronic devices may not be as high as silicon based on electronic devices, but our emphasis is on the functionalities that silicon and other type of materials do not possess. Therefore, the applications of piezotronics, pieozo-phototronic and piezo-photonics are complimentary to those of silicon technologies, so that they can be integrated for smart systems [48].

Acknowledgements

Research was supported by DARPA (Army/AMCOM/REDSTONE AR, W31P4Q-08-1-0009), BES DOE (DE-FG02-07ER46394), KAUST Global Research Partnership, and NSF (DMS0706436, CMMI

0403671). We thank the contributions made by Drs. Zhiyuan Gao, Yaguang Wei, Cheng Li, Jinhui Song, Peng Fei, Yudong Gu, Zhou Li, Guang Zhu and Yue Shen.

References

[1] Z.L. Wang, Mater. Sci. Eng. R 64 (2009) 3.
[2] S.J. Pearton, W.T. Lim, J.S. Wright, L.C. Tien, H.S. Kim, D.P. Norton, H.T. Wang, B.S. Kang, F. Ren, J. Jun, J. Lin, A. Osinsky, J. Electron. Mater. 37 (2008) 1426.
[3] M.H. Huang, Y. Wu, H. Feick, N. Tran, E. Weber, P. Yang, Adv. Mater. 13 (2001) 113.
[4] Z.W. Pan, Z.R. Dai, Z.L. Wang, Science 209 (2001) 1947.
[5] Z.R. Dai, Z.W. Pan, Z.L. Wang, Adv. Funct. Mater. 13 (2003) 9.
[6] X.Y. Kong, Z.L. Wang, Nano Lett. 3 (2003) 1625.
[7] X.Y. Kong, Z.L. Wang, Appl. Phys. Lett. 84 (2004) 975.
[8] P.X. Gao, Y. Ding, W.J. Mai, W.L. Hughes, C.S. Lao, Z.L. Wang, Science 309 (2005) 1700.
[9] X.Y. Kong, Y. Ding, R.S. Yang, Z.L. Wang, Science 303 (2004) 1348.
[10] R.S. Yang, Y. Ding, Z.L. Wang, Nano Lett. 4 (2004) 1309.
[11] Y. Xi, J.H. Song, S. Xu, R.S. Yang, Z.Y. Gao, C.G. Hu, Z.L. Wang, J. Mater. Chem. 19 (2009) 9260.
[12] Z.Y. Gao, Y. Ding, S.S. Lin, Y. Hao, Z.L. Wang, Phys. Status Solidi RRL 3 (2009) 260.
[13] Z. Li, R.S. Yang, M. Yu, F. Bai, C. Li, Z.L. Wang, J. Phys. Chem. C 112 (2009) 20114.
[14] M.H. Huang, S. Mao, H. Feick, H.Q. Yan, Y.Y. Wu, H. Kind, E. Weber, R. Russo, P.D. Yang, Science 292 (2001) 1897.
[15] X.W. Sun, J.Z. Huang, J.X. Wang, Z.A. Xu, Nano Lett. 8 (2008) 1219.
[16] X.M. Zhang, M.Y. Lu, Y. Zhang, L.J. Chen, Z.L. Wang, Adv. Mater. 21 (2009) 2767.
[17] M. Law, L.E. Greene, J.C. Johnson, R. Saykally, P.D. Yang, Nat. Mater. 4 (2005) 455.
[18] X.D. Wang, J. Zhou, C.S. Lao, J.H. Song, N.S. Xu, Z.L. Wang, Adv. Mater. 19 (2007) 1627.
[19] J. Zhou, Y.D. Gu, Y.F. Hu, W.J. Mai, P.H. Yeh, G. Bao, A.K. Sood, D.L. Polla, Z.L. Wang, Appl. Phys. Lett. 94 (2009) 191103.
[20] E. Comini, G. Faglia, G. Sberveglieri, Z. Pan, Z.L. Wang, Appl. Phys. Lett. 81 (2002) 1869.
[21] E. Comini, C. Baratto, G. Faglia, M. Ferroni, G. Sberveglieri, J. Phys. D: Appl. Phys. 40 (2007) 7255.
[22] B. Weintraub, Y.G. Wei, Z.L. Wang, Angew. Chem. 48 (2009) 8981.
[23] Z.L. Wang, J.H. Song, Science 312 (2006) 242.
[24] X.D. Wang, J.H. Song, J. Liu, Z.L. Wang, Science 316 (2007) 102.
[25] Z.L. Wang, Adv. Funct. Mater. 18 (2008) 3553.
[26] Z.L. Wang, Mater. Today 10 (2007) 20.
[27] Y. Qin, X.D. Wang, Z.L. Wang, Nature 451 (2008) 809.
[28] Y.F. Lin, J.H. Song, Y. Ding, S.Y. Liu, Z.L. Wang, Appl. Phys. Lett. 92 (2008) 022105.
[29] M.Y. Lu, J.H. Song, M.P. Lu, C.Y. Lee, L.J. Chen, Z.L. Wang, ACS Nano 3 (2009) 357.
[30] R.S. Yang, Y. Qin, L.M. Dai, Z.L. Wang, Nat. Nanotechnol. 4 (2009) 34.
[31] J. Zhou, P. Fei, Y.D. Gu, W.J. Mai, Y.F. Gao, R.S. Yang, G. Bao, Z.L. Wang, Nano Lett. 8 (2008) 3973.
[32] J. Zhou, Y.D. Gu, P. Fei, W.J. Mai, Y.F. Gao, R.S. Yang, G. Bao, Z.L. Wang, Nano Lett. 8 (2008) 3035.
[33] Y.F. Gao, Z.L. Wang, Nano Lett. 7 (2007) 2499.
[34] Y.F. Gao, Z.L. Wang, Nano Lett. 9 (2009) 1103.
[35] Z.Y. Gao, J. Zhou, Y.D. Gu, P. Fei, Y. Hao, G. Bao, Z.L. Wang, J. Appl. Phys. 105 (2009) 113707.
[36] R.S. Yang, Y. Qin, C. Li, G. Zhu, Z.L. Wang, Nano Lett. 9 (2009) 1201.
[37] R.S. Yang, Y. Qin, L.M. Dai, Z.L. Wang, Appl. Phys. Lett. 94 (2009) 022905.
[38] S. Xu, Y.G. Wei, M. Kirkham, J. Liu, W.J. Mai, D. Davidovic, R.L. Snyder, Z.L. Wang, J. Am. Chem. Soc. 130 (2008) 14958.
[39] X.D. Wang, E. Graugnard, J.S. King, Z.L. Wang, C.J. Summers, Nano Lett. 4 (2004) 2223.
[40] Y. Qin, R.S. Yang, Z.L. Wang, J. Phys. Chem. C 112 (2008) 18734.
[41] S. Xu, Y. Ding, Y.G. Wei, H. Fang, Y. Shen, A.K. Sood, D.L. Polla, Z.L. Wang, J. Am. Chem. Soc. 131 (2009) 6670.
[42] S. Xu, Y. Qin, C. Xu, Y.G. Wei, R.S. Yang, Z.L. Wang, Nat. Nanotechnol. (2010), online.
[43] Z.Y. Fan, J.G. Lu, Appl. Phys. Lett. 86 (2005) 032111.
[44] Y.F. Hu, Y. Zhang, Y.L. Chang, R.L. Snyder, Z.L. Wang, ACS Nano (2010), doi:10.1021/nn1010045.
[45] Y.F. Hu, Y.L. Chang, P. Fei, R.L. Snyder, Z.L. Wang, ACS Nano 4 (2010) 1234.
[46] C.T. Huang, J.H. Song, W.F. Lee, Y. Ding, Z.Y. Gao, Y. Hao, L.J. Chen, .L. Wang, J. Am. Chem. Soc. 132 (2010) 4766.
[47] C.T. Huang, J.H. Song, C.M. Tsai, W.F. Lee, D.H. Lien, Z.Y. Gao, Y. Hao, L.J. Chen, Adv. Mater. (in press).
[48] Z.L. Wang, J. Phys. Chem. Lett. 1 (2010) 1388.